Dendritic sidebranches of a binary system with enforced flow*

Li Xiang-Ming(李向明) and Wang Zi-Dong(王自东)†

School of Materials Science and Engineering, University of Science and Technology Beijing, Beijing 100083, *China*

(Received 19 March 2010; revised manuscript received 23 June 2010)

In the present paper, the problem of sidebranches in the binary dendritic growth with enforced flow is studied. The positions of the first sidebranch and spacing of dendritic sidebranches are presented. For the neutral stable mode of dendritic growth, effects of various parameters on sidebranches are analysed. Our result shows that sidebranches are produced behind a critical point $\xi'_{\rm C}$.

Keywords: binary system, sidebranches, enforced flow, pattern formation

PACC: 6470D, 6630J, 4725Q, 8130D

1. Introduction

Dendrites are the most common pattern of solidification microstructures.[1−7] It virtually always appears in the manufacture of alloy castings, ingots and weldments. Experimental observation shows that dendrite consists of the smooth tip and sidebranches.[1,5] Exploring the essence and origin of such phenomena has great theoretical and practical significance.

The microscopic solvability theory[8−11] states that anisotropy of surface tension is a necessary condition for steady needle growth; sidebranching structure of dendrite is induced by continuously acting thermal fluctuation or noise forced at the tip of the steady needle solution.[12,13] However, the interfacial wave theory[14−21] of dendritic growth shows that the problem of the selection and pattern formation of the dendrite cannot be separated; any initial perturbation which is probable the thermal fluctuation or the outer disturbance can induce the formation of continuous train of sidebranches. The discussions of the common points and differences between the microscopic solvability theory and interfacial wave theory can be found in Ref. [19].

Following interfacial wave theory, for the case of isotropic surface tension, the dendritic growth may be described by a time-periodic solution: the so-called neutrally global trapped wave mode. In the dynamical system of dendritic growth there exists a simple turning point in the complex plane.[15] The turning point plays a crucial role for the formation of dendritic structure. Due to the existence of singularity points, Xu[15] divided the whole complex plane into three regions: the outer region, the turning point region, and the dendritic tip inner region. Then he found and matched all the solutions and finally obtained the global mode solution.[16−18] Interfacial wave theory shows that perturbations arising near the tip propagate along dendritic interface and undergo amplification, resulting in the ultimate development of visible sidebranches some distance away from the dendritic tip.

We have obtained the uniformly valid asymptotic solution of the binary dendritic growth with enforced flow, and presented the selection criterion.[20,21] In the present paper, we will describe the sidebranching problem taking into account three-dimensional axisymmetric shape of dendritic growth with isotropic surface tension and analyse effects of undercooling, solute and forced flow on dendritic sidebranches.

2. Model and solution of neutral mode

We consider a system of free dendritic growth in a binary system which is undercooled to a temperature T_∞ below the interfacial equilibrium temperature $T_{\rm I}$. At for infinite upstream, an external flow with velocity U_∞ is forced to run opposite direction of the dendritic growth. The temperature fields T_j $(j = {\rm L}, {\rm S})$ and

*Project supported by the High Technology Research and Development Programme of China (Grant No. 2007AA03Z108).

†Corresponding author. E-mail: wangzd@mater.ustb.edu.cn

© 2010 Chinese Physical Society and IOP Publishing Ltd

concentration fields C_i satisfy the partial differential equations:

$$\frac{\partial T_{\rm L}}{\partial t} + \boldsymbol{U}\cdot\boldsymbol{\nabla} T_{\rm L} = \kappa_{\rm L}\boldsymbol{\nabla}^2 T_{\rm L}, \tag{1}$$

$$\frac{\partial T_{\rm S}}{\partial t} = \kappa_{\rm S}\boldsymbol{\nabla}^2 T_{\rm S}, \tag{2}$$

$$\frac{\partial C_{\rm L}}{\partial t} + \boldsymbol{U}\cdot\boldsymbol{\nabla} C_{\rm L} = D_{\rm L}\boldsymbol{\nabla}^2 C_{\rm L}, \tag{3}$$

$$\frac{\partial C_{\rm S}}{\partial t} = D_{\rm S}\boldsymbol{\nabla}^2 C_{\rm S}, \tag{4}$$

where subscripts L and S designate the liquid and the solid, κ_j and D_j are the thermal diffusivity and the mass diffusivity in the j-phase, respectively. The velocity field in the liquid phase $\boldsymbol{U}$ meets the Navier–Stokes equation

$$\frac{\partial \boldsymbol{U}}{\partial t} + \boldsymbol{U}\cdot\boldsymbol{\nabla}\boldsymbol{U} = -\frac{1}{\rho}\boldsymbol{\nabla} P + \nu\boldsymbol{\nabla}^2\boldsymbol{U}, \tag{5}$$

and

$$\boldsymbol{\nabla}\cdot\boldsymbol{U} = 0, \tag{6}$$

where P is the pressure, ν is the kinematic viscosity of the liquid, ρ is the density of the melt. Here we assume that the convection in the melt is only induced by the forced flow, so the solidification system contains no density change and gravity.

To complete the specification of this model, we introduce the boundary condition at the interface[15,21]

$$T_{\rm I} = T_{\rm L} = T_{\rm S} = T_{\rm M}\left(1 - \frac{K\gamma}{\Delta H}\right) + mC_{\rm L}, \tag{7}$$

$$\Delta H V_{\rm I} = k_{\rm S}\boldsymbol{n}\cdot\boldsymbol{\nabla} T_{\rm S} - k_{\rm L}\boldsymbol{n}\cdot\boldsymbol{\nabla} T_{\rm L}, \tag{8}$$

$$(1-\kappa)\, C_{\rm L} V_{\rm I} = D_{\rm S}\boldsymbol{n}\cdot\boldsymbol{\nabla} C_{\rm S} - D_{\rm L}\boldsymbol{n}\cdot\boldsymbol{\nabla} C_{\rm L}, \tag{9}$$

$$C_{\rm S} = \kappa C_{\rm L}, \tag{10}$$

$$\boldsymbol{U}\cdot\boldsymbol{n} = 0, \tag{11}$$

$$\boldsymbol{U}\cdot\boldsymbol{\tau} = 0, \tag{12}$$

where K is the curvature operator, γ is the coefficient of surface tension, m is the slope of the liquidus, $T_{\rm M}$ stands for the equilibrium melting temperature of the solvent material, ΔH is the latent heat, k_j $(j = {\rm L}, {\rm S})$ is the thermal conductivity in j-phase, κ is the distribution coefficient and $V_{\rm I}$ is the normal velocity of interface, $\boldsymbol{n}$ and $\boldsymbol{\tau}$ are respectively the unit normal and tangent vectors to the interface of the dendrite. Equation (7) is the Gibbs–Thomson condition, and equations (8) and (9) describe the conservation of energy and solute mass, respectively; equation (10) is the segregation condition for the solute, and the last two equations are conditions of velocity at the interface.

For the system of dendritic growth, Eqs. (1)–(12), we can adopt the paraboloidal coordinate system (ξ, η, φ), which moves with dendritic interface. The mathematical formulation in (ξ, η, φ) has been given in Ref. [21], where we measure all lengths in units of solute diffusion length $l_{\rm D} = D_{\rm L}/V$ and all times in unit of $l_{\rm D}/V$, where V is the growth velocity of dendritic tip. By using the matched asymptotic method and multiple variable expansion approach,[17,18] we have obtained the analytical solution of the system. In the paraboloidal coordinate system (ξ, η, φ), the shape of dendritic interface corresponding to a neutral mode can be written in the form

$$\eta_{\rm S}(\xi, t) = 1 + \varepsilon_*^2\eta_1(\xi, t) + \frac{\tilde{\mu}_0(\varepsilon_*)}{\eta_0^2}\tilde{h}_0(\xi) \times \exp\left(\mathrm{i}\frac{{\rm Im}(\sigma)t}{\varepsilon_*\eta_0^2}\right) + \cdots, \tag{13}$$

where ${\rm Im}(\sigma)$ is the imaginary part of the complex eigenvalue $\sigma = \sigma_0 + \varepsilon_*\sigma_1$, ε_* is the stability critical number, η_0 is a constant and $\tilde{\mu}_0(\varepsilon) = 0.0001 \ll 1$.

The first term on the right-hand side of Eq. (13) is the Ivantsov's solution[22] for the case without surface tension. The second term represents the first order approximation of the basic solution with isotropic surface tension, which has no influence on the linear stability analysis of the dendritic growth. The third term is the unsteady perturbed solution of the neutrally stable mode. The normal mode solution $\tilde{h}_0(\xi)$ can be given as, for $0 < \xi < \xi_{\rm C}'$,

$$\tilde{h}_0(\xi) = \exp\left(\frac{\mathrm{i}}{\varepsilon_*}\int_{\xi_{\rm C}}^{\xi}\bar{k}_0^{(1)}(\xi)\mathrm{d}\xi\right) + \exp\left(\frac{\mathrm{i}}{\varepsilon_*}\int_{\xi_{\rm C}}^{\xi}\bar{k}_0^{(3)}(\xi)\mathrm{d}\xi\right); \tag{14}$$

as $\xi_{\rm C}' < \xi$,

$$\tilde{h}_0(\xi) = \exp\left(\frac{\mathrm{i}}{\varepsilon_*}\int_{\xi_{\rm C}}^{\xi}\bar{k}_0^{(3)}(\xi)\mathrm{d}\xi\right). \tag{15}$$

Here $\bar{k}_0^{(1)}$ and $\bar{k}_0^{(3)}$ are the wave-number functions which satisfy the dispersion relation,[21] and $\xi_{\rm C}'$ is the intersection point of anti-Stokes line A_2 with the real axis of ξ.[15] The quantization condition for the selection of dendritic growth with forced flow is

$$\frac{1}{\varepsilon}\int_0^{\xi_{\rm C}}\left(\bar{k}_0^{(1)} - \bar{k}_0^{(3)}\right)\mathrm{d}\xi = \left(2n + 1 + \frac{1}{2} + \frac{\theta_0}{2}\right)\pi - \frac{\mathrm{i}}{2}\ln\alpha_0, \quad (n = 0, \pm1, \pm2, \ldots), \tag{16}$$

where $\alpha_0 \exp(\mathrm{i}\theta_0\pi) = \bar{k}_0^{(1)}(0)/\bar{k}_0^{(3)}(0)$. The singularity point ξ_{C} meets

$$\sigma_0 = \sqrt{\frac{4\Lambda_1}{27}} \left(\frac{1-\mathrm{i}\xi_{\mathrm{C}}}{1+\mathrm{i}\xi_{\mathrm{C}}}\right)^{3/4}. \tag{17}$$

ε and Λ_1 are the parameters.[21]

3. Numerical results

From Eqs. (13)–(15), it is seen that if the critical number ε_* and $\mathrm{Im}(\sigma)$ can be fixed, then the interfacial solution for the neutral mode can be determined. While the quantization condition (15) shows that ε_* and $\mathrm{Im}(\sigma)$ are the only functions of undercooling, solute concentration, and the velocity of forced flow. Hence, for these fixed growth conditions, values of ε_* and $\mathrm{Im}(\sigma)$ can be uniquely determined. Due to the complexity of the interfacial solution above, we can use numerical calculation methods[23] to analyse and determine the shape and position of sidebranches. Using Gauss–Legendre integral method and Newton's iterative method, we have carried out a number of numerical calculations for the neutrally stable mode of dendritic growth under various growth conditions. The physical quantities and their data for SCN-acetone used in the calculations are given in Table 1.[24,25] In order to show the physical situation of sidebranching easily, we return to the dimensional length scale. In our calculations, we assume that the thermal diffusivity in the liquid phase κ_{L} is equal to that of solid κ_{S}, and the diffusion of solute in the solid is negligible.

Table 1. Physical parameter for SCN-acetone.[24,25]

melting temperature $T_{\mathrm{M}} = 331.23$ K
latent heat $\Delta H = 47.51$ J/cm^3
specific heat $c_{\mathrm{p}} = 2$ J/g $\cdot$ K
density of melt $\rho = 0.982$ g/cm^3
thermal diffusivity of liquid $\kappa_{\mathrm{L}} = 1.14 \times 10^{-3}$ cm^2/s
mass diffusivity of liquid $D_{\mathrm{L}} = 1.27 \times 10^{-5}$ cm^2/s
isotropic surface tension $\gamma = 0.91 \times 10^{-6}$ J/cm^2
distribution coefficient $\kappa = 0.1$
kinematic melt viscosity $\nu = 2.68 \times 10^{-2}$ cm^2/s
slope of the liquidus $m = -2.8$ K(wt%)$^{-1}$

The point ξ'_{C} plays a very important role in the formation of dendritic shape, which has been explained in Ref. [15]. Here we fix the position of ξ'_{C}. The position of point ξ'_{C} at the interface is a function of undercooling $\Delta T = T_{\mathrm{M}} + mC_\infty - T_\infty$, the Reynolds number $Re = U_\infty l_{\mathrm{C}}/\nu$ and the morphological number $M = -mC_\infty c_{\mathrm{P}}\rho/\Delta H$, where m is the slope of liquidus, $l_{\mathrm{C}} = \gamma c_{\mathrm{P}}\rho T_{\mathrm{M}}/(\Delta H)^2$ is the capillary length and C_∞ is the solute concentration. We present the variation of distance from ξ'_{C} to dendritic tip with ΔT and Re for SCN-0.064-wt% acetone in Fig. 1. It is noted that the distance is measured with respect to the axial centreline of the dendrite, which is denoted by "$\mathrm{L_0}$", as shown in Fig. 2. It is seen that the distance decreases with ΔT and Re.

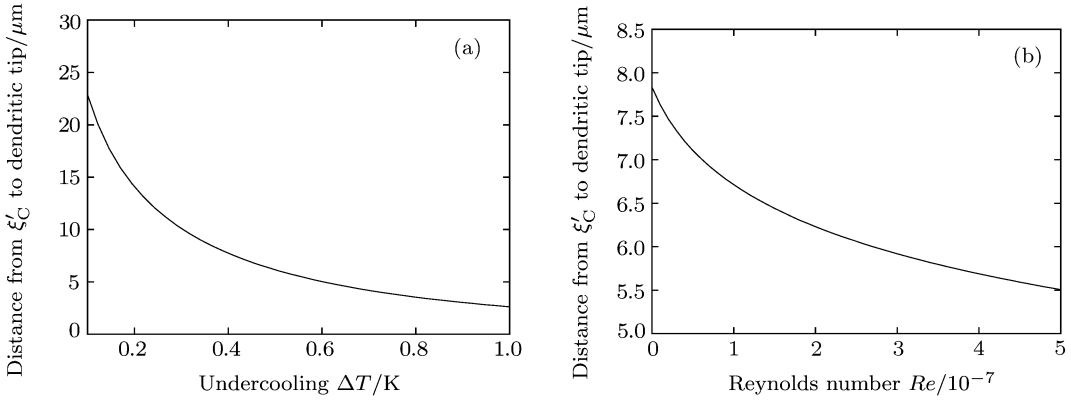


Fig. 1. The variation of distance from ξ'_{C} to dendritic tip with (a) ΔT at $Re = 5 \times 10^{-7}$; (b) Re at $\Delta T = 0.5$ K for the SCN-0.064-wt% acetone.

In Fig. 2 we present the dendritic shape of SCN containing 0.064-wt% acetone on the $Y = 0$ plane in Cartesian coordinate system (X, Y, Z) at $t = 0$, $\Delta T = 0.5076$ K and $Re = 5 \times 10^{-7}$. Solid curve is our result, and dotted curve is for the Ivantsov's interface.[22] The first sidebranch is defined as the first protrusion, from which to dendritic tip the distance is denoted as "$\mathrm{L_t}$" showed in Fig. 2. Sidebranch spacing which is the interval between neighbouring sidebranches is denoted as "$\mathrm{L_s}$".

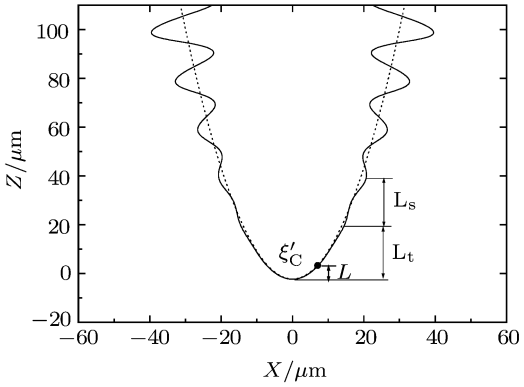


Fig. 2. Projection of dendritic interface on $Y = 0$ plane in the Cartesian coordinate system (X, Y, Z) for $t = 0$, $\Delta T = 0.5092$ K, $Re = 5 \times 10^{-7}$.

Figure 2 shows that sidebranches are produced behind a critical point ξ'_C. The amplitude of sidebranches exponentially increases as a function of the distance from the dendritic tip, which is in agreement with the experimental observation.[1,5]

Results of numerical calculations about the characteristic lengths of sidebranches are shown in Figs. 3 and 4 for SCN-0.064-wt% acetone at $t = 0$. In Figs. 3, we show the variation of distance from sidebranch-tip to dendritic tip with increasing undercooling and Reynolds number. The solid, dashed, dotted, and dot dashed curves denote the distances from the first, the second, the third, and the fourth sidebranch-tip to dendritic tip, respectively. Figure 3(a) shows that the distance decreases with ΔT for fixed $Re = 5 \times 10^{-8}$. For smaller undercooling, the distance decreases rapidly as undercooling increases, but for larger undercooling, the variation changes slowly. Figure 3(b) shows the variation of distance with the forced flow for $\Delta T = 0.5092$ K. The distance also decreases as Re increases.

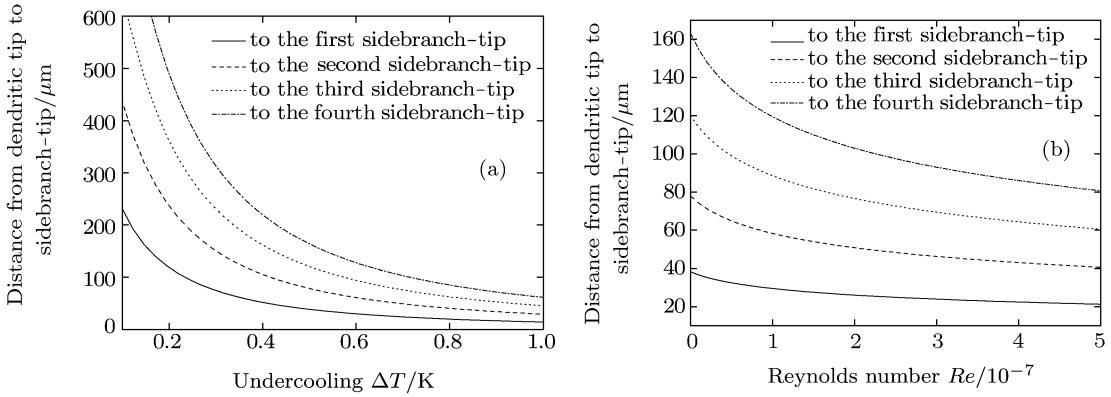


Fig. 3. Variation of the distance from sidebranch-tip to dendritic tip (a) with ΔT at $Re = 5 \times 10^{-8}$; (b) with Re at $\Delta T = 0.5092$ K for SCN-0.064-wt% acetone.

Similar results for the sidebranch spacing as a function of undercooling and the Reynolds number are given in Fig. 4. The solid curve is the spacing between the first and the second sidebranches, so called the first spacing; the dashed and dotted curves correspond to the second and the third spacings, respectively. Figure 4(a) shows that spacing decreases as undercooling increases for fixed $Re = 5 \times 10^{-8}$; the changing is more obvious in the region of small undercooling. It is also seen that the three curves have small differences in the regime of small undercooling; for a fixed undercooling, the second spacing which is smaller than the third spacing is larger than the first one. However, in the regime of larger undercooling the three curves almost coincide. That is to say, for larger undercooling, the three sidebranch spacings are nearly the same. The change of spacing with undercooling is qualitatively in good agreement with the experimental observation of pure material SCN given by Corrigan *et al.*[26] Figure 4(b) shows that the sidebranch spacing decreases as Re increases. For the fixed forced flow, the spacing gets far away from the dendritic tip.

From Fig. 3(b) we can also see that the position of the first sidebranch with the forced flow is closer to dendritic tip than the one without the forced flow. While figure 4(b) shows that sidebranch spacing of the dendrite with the forced flow is smaller than the one without forced flow. Hence, we can predict that the external forced flow induces more sidebranches, which is in agreement with the result of phase field simulation.[7]

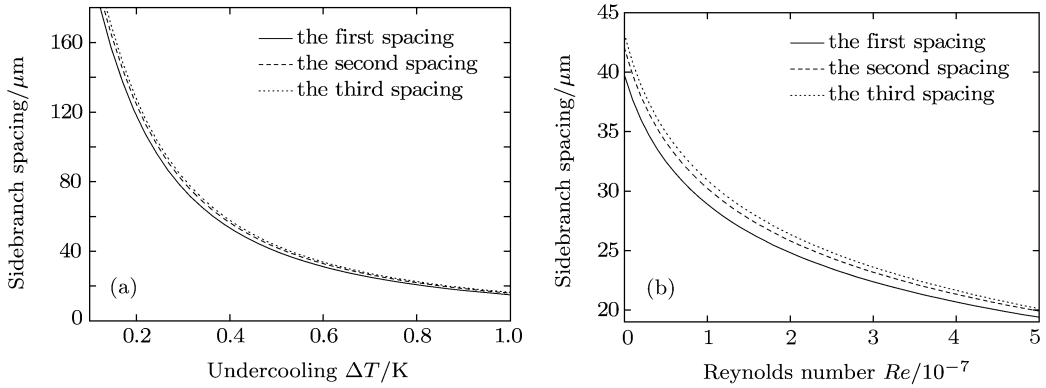


Fig. 4. The variation of sidebranch spacing (a) with ΔT at $Re = 5 \times 10^{-8}$; (b) with Re at $\Delta T = 0.5092$ K for SCN-0.064-wt% acetone.

In Figs. 5 we give the variation of position and spacing of sidebranches with solute concentration C_∞ at $t = 0$, $\Delta T = 0.5092$ K and $Re = 5 \times 10^{-8}$. It is seen that both of the distances from sidebranch-tip to dendritic tip, and between spacings decrease obviously for small M.

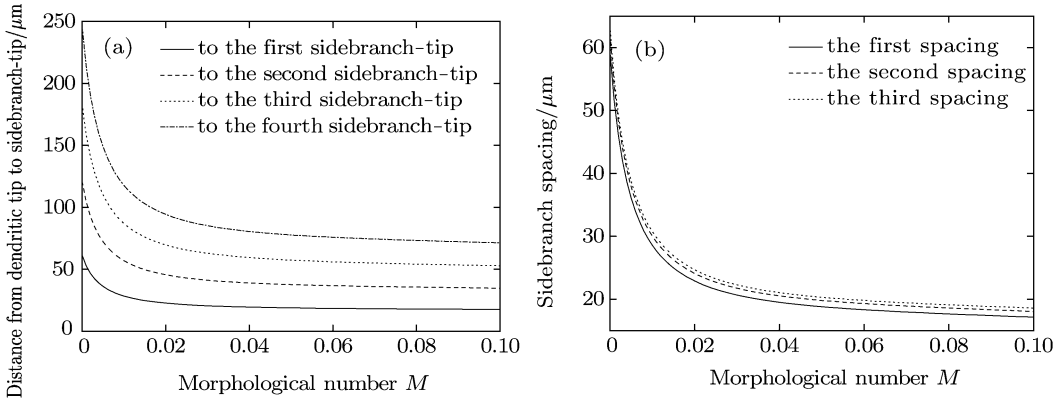


Fig. 5. The variation of (a) distance from sidebranch-tip to dendritic tip and (b) sidebranch spacing with M at $\Delta T = 0.5092$ K and $Re = 5 \times 10^{-8}$.

4. Conclusions

This paper is concerned with sidebranches of binary dendritic growth with enforced flow. We have numerically solved the solution of dendritic shape corresponding to a neutral mode. Effects of undercooling, solute concentration and forced flow on sidebranches have been presented. Our numerical calculations show that the distance from sidebranch-tip to dendritic tip and sidebranch spacing decrease as undercooling and the Reynolds number increase. Furthermore, changes of these characteristic lengths are obviously in the regions of small undercooling and solute concentration. Forced flow can induce more sidebranches. Our results are in agreement with the experimental observation and related phase field simulation.

References

[1] Hurle D J T ed. 1993 *Handbook of Crystal Growth*, Vol. 1: *Fundamental*, Part B: *Transport and Stability* (Amsterdam: Elsevier)

[2] Chen M W, Lan M, Wang Y Y, Wang Z D, Xu J J and Yuan L 2009 *Chin. Phys.* B **18** 1691

[3] Cai L C and Xi F 2009 *Chin. Phys.* B **18** 2898

[4] Chen M W, Wang Z D and Sun R J 2007 *Acta Phys. Sin.* **56** 1819 (in Chinese)

[5] Kessler D A, Koplik J and Levin H 1988 *Adv. Phys.* **37** 255

[6] Wang J C, Wang Z J and Yang G C 2008 *Acta Phys. Sin.* **57** 1246 (in Chinese)

[7] Lan C W and Shih C J 2004 *J. Cryst. Growth* **264** 472

[8] Ben Amar M and Pomeau Y 1986 *Europhys. Lett.* **2** 307

[9] Barbieri A, Hong D C and Langer J S 1987 *Phys. Rev.* A **35** 1802
[10] Kessler D A and Levine H 1986 *Phys. Rev. Lett.* **57** 3069
[11] Kessler D, Koplik J and Levine H 1988 *Adv. Phys.* **37** 255
[12] Barber M N, Barbieri A and Langer J S 1987 *Phys. Rev.* A **36** 3340
[13] Langer J S 1987 *Phys. Rev.* A 36 3350
[14] Xu J J 1991 *Phys. Rev.* A **43** 930
[15] Xu J J 1997 *Interfacial Wave Theory of Pattern Formation: Selection of Dendrite and Viscous Fingering in a Hele-Shaw Flow* (New York: Springer) pp. 125–213
[16] Xu J J 2000 *Dynamical Theory of Dendritic Growth in Convective Flow* (New York: Springer) pp. 131–231
[17] Chen Y Q, Tang X X and Xu J J 2009 *Chin. Phys.* B **18** 671
[18] Chen Y Q, Tang X X and Xu J J 2009 *Chin. Phys.* B **18** 685
[19] Xu J J and Yu D S 1999 *J. Cryst. Growth* **198–199** 43
[20] Li X M, Chen M W and Wang Z D 2008 *J. Univ. Sci. Technol. Beijing* **30** 652 (in Chinese)
[21] Li X M, Wang Z D and Wang Q Y 2009 *J. Appl. Phys.* **106** 053511
[22] Ivantsov G P 1947 *Dokl. Akad. Nauk SSSR* **58** 567
[23] Hoffman J D 1992 *Numerical Methods for Engineers and Scientists* (New York: Marcel Dekker, Inc.) pp. 1–320
[24] Liu Y C, Roux B and Lan C W 2007 *Int. J. Heat Mass Trans.* **50** 5031
[25] Yasuda H, Ohnaka I, Yano T and Tanaka H 1996 *ISIJ Int.* **36** S167
[26] Corrigan D P, Koss M B, LaCombe J C, de Jager K D, Tennenhouse L A and Glicksman M E 1999 *Phys. Rev.* E **60** 7217